Dynamic phases, clustering, and chain formation for driven disk systems in the presence of quenched disorder

Y. Yang,[1,2] D. McDermott,[1,2] C. J. Olson Reichhardt,[1] and C. Reichhardt[1]
[1]*Theoretical Division, Los Alamos National Laboratory, Los Alamos, New Mexico 87545, USA*
[2]*Department of Physics, Wabash College, Crawfordsville, Indiana 47933, USA*
(Received 15 August 2016; published 10 April 2017)

We numerically examine the dynamic phases and pattern formation of two-dimensional monodisperse repulsive disks driven over random quenched disorder. We show that there is a series of distinct dynamic regimes as a function of increasing drive, including a clogged or pile-up phase near depinning, a homogeneous disordered flow state, and a dynamically phase separated regime consisting of high-density crystalline regions surrounded by a low density of disordered disks. At the highest drives the disks arrange into one-dimensional moving chains. The phase separated regime has parallels with the phase separation observed in active matter systems, but arises from a distinct mechanism consisting of the combination of nonequilibrium fluctuations with density-dependent mobility. We discuss the pronounced differences between this system and previous studies of driven particles with longer-range repulsive interactions moving over random substrates, such as superconducting vortices or electron crystals, where dynamical phase separation and distinct one-dimensional moving chains are not observed. Our results should be generic to a broad class of systems in which the particle-particle interactions are short ranged, such as sterically interacting colloids or Yukawa particles with strong screening driven over random pinning arrays, superconducting vortices in the limit of small penetration depths, or quasi-two-dimensional granular matter flowing over rough landscapes.

DOI: 10.1103/PhysRevE.95.042902

I. INTRODUCTION

A wide range of systems can be effectively modeled as a collection of repulsively interacting particles that are coupled to a substrate that serves as quenched disorder, and these systems typically exhibit a transition from a pinned to a sliding state under an applied external driving force [1]. Examples of such systems include vortices in type-II superconductors [2–6], driven electron or Wigner crystals [7–9], skyrmions in chiral magnets [10,11], charge stabilized colloids [12–14], and magnetically interacting colloidal systems [15,16]. The depinning transition can either be elastic, where the particles keep their same neighbors, or plastic, where the particles exchange neighbors and break apart [1,3]. In systems with intermediate or long-range repulsive particle-particle interactions, the ground state is usually a defect-free triangular lattice. When plastic depinning occurs, pinned and mobile particles coexist, leading to a proliferation of topological defects in the lattice and producing highly disordered particle configurations during plastic flow [1–3]. At higher drives there can be a transition from the plastic flow state to a moving anisotropic crystal [3,17,18] or moving smectic state [19–22]. This transition is associated with an increase in the ordering of the system and produces a distinct change in the structure factor [20–22] and the density of topological defects [20,22] as well as cusps or dips in the transport curves and changes in the fluctuation spectra [22–24]. Depending on the dimensionality and anisotropy of the system, these dynamical transitions can have continuous or first order characteristics [1,3,25].

In most of the systems where depinning and sliding dynamics have been studied, the repulsive particle-particle interactions are modeled as a smooth potential that is either long range, as in the case of Coulomb or logarithmic interactions, or screened long range, such as a Bessel function interaction for superconducting vortices or a Yukawa interaction for colloidal systems. There are many systems where the repulsive particle-particle interactions are short range with sharp cutoffs, such as sterically interacting colloids [26,27], emulsions [28], micelles [29], binary fluids [30], bubble rafts [31–33], granular matter [34,35], charged colloids under strong screening [36,37], and solid state systems under certain conditions. For most of these systems it should be possible to flow the particles over some type of rough surface or landscape.

Systems with sharp repulsive interaction cutoffs, such as hard disks, can exhibit very different behavior from systems with long-range repulsion, such as a strong density dependence of the response near a crystallization or jamming transition [35,38]. Two-dimensional (2D) systems with long-range repulsive interactions form an ordered solid down to very low densities since the particles are always within interaction range of each other, whereas hard-disk systems form a crystalline solid only for the density at which the particles can just touch each other, which corresponds to a packing density or area coverage of $\phi = 0.9$ for 2D monodisperse nonfrictional disk packings [35]. For densities below the crystallization density, the hard-disk system forms a disordered or liquidlike state. It is not clear whether a hard-disk assembly driven over random disorder would exhibit the same types of dynamical transitions observed in systems with longer-range interactions such as superconducting vortices, Wigner crystals, skyrmions, and charged colloids, or whether it would simply form a moving disordered state at high drives. Previous studies addressed how pinning and obstacles affect the onset of the jamming transition in bidisperse disk packs [39,40]; however, the driven dynamics for nonzero loading above the jammed state have not been studied. Although it may seem that hard disks driven over quenched disorder would simply exhibit the same general dynamics, such as dynamical reordering at high drives, as repulsive particle systems with longer-range interactions, the question has surprisingly not previously been addressed.

Here we examine an assembly of monodisperse harmonically interacting repulsive disks driven over a random array of pinning sites. We focus on disk densities $\phi < 0.9$, below jamming or crystallization. Despite the apparent simplicity of the model, we find that this system exhibits dynamical phases distinct from those observed in studies of longer-range repulsive particles driven over random disorder. When the number of pinning sites is smaller than the number of disks, the pinned phase is associated with a pile up or clogging phenomenon in which the system breaks up into clumps or clusters, with unpinned disks prevented from moving by interactions with disks trapped at pinning sites. As the drive is increased beyond depinning, the system enters either a fluctuating uniform disordered state or a phase separated cluster state consisting of a low-density gas of disks coexisting with high-density clusters. Within the clusters, the disks form a predominantly triangular lattice. The phase separated states generally appear when the driving force is close to the value of the maximum pinning force. For even higher drives, the system can transition into a collection of one-dimensional (1D) moving chains, and the structure factor exhibits a strong smectic ordering signature. We characterize the different phases and the transitions between them using velocity-force curves, the transverse root mean square displacements, the structure factor, and the density of non-sixfold coordinated particles.

Dynamical phase separation does not normally occur in systems with longer-range interactions since the coexistence of a high-density and a low-density phase would have a prohibitively large energy cost due to the close spacing of the particles in the dense phase. For the disk system, the energy cost of the particle-particle interactions is zero until the disks come into contact, which occurs only at the highest densities. Similarly, strong 1D chain formation occurs when the disks can approach each other very closely in the direction of the applied drive without overlapping. It is known that 2D granular systems that undergo inelastic collisions can exhibit cluster instabilities [41,42]; however, in our system there are no frictional contacts between the disks. The density phase separated regime has parallels with an active matter clustering effect, and arises when the combination of disk-disk collisions and pinning produce nonequilibrium transverse fluctuations of the disks as well as a density-dependent mobility. Studies of active matter systems with short-range particle-particle repulsion and density-dependent mobility show similar clustering behavior [43–46]. At higher drives for the disk system, we find that a uniform moving state forms when the transverse diffusion is lost. We also find that at the higher drives, the disks align in nearly 1D chains in which the disk spacing is nearly zero in the longitudinal direction but is larger in the transverse direction. Such strong chaining does not occur in systems with longer-range repulsive interactions since the high particle density along the 1D chains would impose a prohibitively high energy cost. Due to the short-range interactions in the disk system, the disks incur no energy penalty when they form 1D chains.

Our work suggests that dynamical phase separation and chain formation are general features of driven systems with short-range or hard-disk particle-particle interactions moving over random disorder. A specific system of this type that could be realized experimentally is sterically interacting colloidal assemblies moving over random disorder. There are already several experiments examining colloidal particles interacting with random pinning [13,14] and periodic pinning [36,37,47,48], and similar studies could be performed for sterically interacting colloids. Other realizations could be achieved using flowing bubble rafts [31–33], where steric interactions come into play, or flowing microemulsions [28,29], where again only short-range interactions arise. Further examples include magnetic bubble systems with weak dipolar interactions or skyrmion systems [11], where at high densities the short-range repulsive core interactions could dominate over the longer-range repulsive interactions. In bulk superconducting vortex systems, the vortex-vortex interactions have a Bessel function form [1,4,6], which decays exponentially for length scales longer than the London penetration depth, so that in certain limits such as at low magnetic fields in samples with very small penetration depths, the vortices could exhibit dynamics similar to those we observe, including the phase separated states. Additionally, there are numerous multiband superconductors in which the vortex interactions are modified and the vortex dynamics is dominated by only short-range repulsive forces [49–51]. There are a wealth of studies of particle-like soft matter systems such as micelles, binary fluids, soft solids, and active matter systems which can be described as having short-range steric interactions. Another class of such systems is assemblies of quasi-2D granular matter flowing over random disorder; however, in these systems additional effects such as friction or inertia can also play a role.

The paper is organized as follows. We provide a description of the model and the numerical simulations in Sec. II. In Sec. III, we describe the different dynamic phases that arise for a fixed amount of quenched disorder when the disk density is varied. At intermediate disk densities, Sec. III A shows that there are three dynamic phases with distinct structure factor signatures that appear as the applied driving force increases: pinned disordered flow, phase separated flow, and a moving chain state. In Sec. III B we discuss the low disk density limit where quasi-1D chaining effects are particularly pronounced. We show in Sec. III C how to categorize the dynamic phases based on the amount of transverse diffusion and topological order. A dynamic phase diagram as a function of driving force and disk density appears in Sec. III D, and we explain how the basic features of the phase diagram can be understood in terms of a drive-dependent dynamic shaking temperature that induces clustering reminiscent of that observed in active matter systems. In Sec. IV we show the evolution of the dynamic phases as a function of increasing disorder strength by first fixing the number of pinning sites while increasing the pinning force, and then fixing the pinning force while increasing the number of pinning sites. In Sec. V we discuss our results in the context of other systems that exhibit depinning phenomena, and in Sec. VI we summarize our work.

II. SIMULATION

We consider a 2D system with an area of L^2 with periodic boundary conditions in the x and y directions. The sample contains N_d harmonically repulsive disks of radius R_d as well as N_p pinning sites that are modeled as nonoverlapping

parabolic potential traps, which can exert a maximum pinning force of F_p on a disk. The disk dynamics are governed by the following overdamped equation of motion:

$$\eta \frac{d\mathbf{R}_i}{dt} = \mathbf{F}_{dd} + \mathbf{F}_p + \mathbf{F}_D. \quad (1)$$

Here η is the damping constant and $\mathbf{R}_i$ is the location of disk i. The disk-disk interaction force is $\mathbf{F}_{dd} = \sum_{i \neq j} k(2R_d - |\mathbf{r}_{ij}|)\Theta(2R_d - |\mathbf{r}_{ij}|)\hat{\mathbf{r}}_{ij}$, where $\mathbf{r}_{ij} = \mathbf{R}_i - \mathbf{R}_j$, $\hat{\mathbf{r}}_{ij} = \mathbf{r}_{ij}/|\mathbf{r}_{ij}|$, the disk radius $R_d = 0.5$, and the spring constant $k = 50$. Distances are measured in simulation units l_0 and forces are measured in simulation units f_0 so that k is in units of f_0/l_0 and the unit of simulation time is $\tau = \eta l_0/f_0$. The pinning force $\mathbf{F}_p$ is modeled as arising from randomly placed parabolic attractive wells with a pinning radius of $r_p = 0.5$, such that only a single disk can be trapped in a given pinning site at a time. F_p is the maximum force exerted by the pinning site at the edge of the well. The driving force $\mathbf{F}_D = F_D\hat{\mathbf{x}}$ is applied along the x direction, and for each driving force we allow at least 1×10^6 simulation time steps to elapse before taking measurements to ensure that the flow has reached a steady state. At each value of F_D we measure the average disk velocity $\langle V_x \rangle = N_d^{-1} \sum_{i=1}^{N_d} \mathbf{v}_i \cdot \hat{\mathbf{x}}$, where $\mathbf{v}_i$ is the instantaneous velocity of disk i. The density ϕ of the system is characterized by the packing fraction or the area covered by the disks, $\phi = N_d \pi R_d^2/L^2$, where $L = 60$ in dimensionless simulation length units. In the absence of disorder, the disks form a polycrystalline state near $\phi \approx 0.85$ and a triangular solid at $\phi \approx 0.9$. A variation of this model was previously used to study the depinning and jamming of bidisperse disks driven over random pinning; in that work, with a disk radii ratio of 1:1.4, the jamming density in a pin free sample was $\phi_j \approx 0.845$ [39].

The main scale determining our choice of parameters is the ratio F_D/F_p of the driving force to the pinning force. When $F_D/F_p \geqslant 1.0$, all the disks are moving. All of the general features of the dynamic phases we observe are robust for varied parameters, and changing F_p simply introduces a linear shift of the phase boundaries. The disk-disk repulsion in our model is harmonic in form, and we choose a large spring constant $k = 50$. For larger values of k, the results are unchanged; however, we must use smaller simulation time steps in order to maintain the numerical stability of our algorithm. The harmonic disk interaction we consider has been used in numerous previous studies to mimic hard disks, particularly for jamming systems [35,38–40]. We note that the model we use is for strictly overdamped systems, whereas in granular matter the role of inertial effects and frictional contacts between grains can be important. We have tested various system sizes and find that our general results are robust.

One example of a soft matter system with a controllable substrate is colloids interacting with optical traps, so a possible experimental realization of our system consists of sterically interacting colloids in the presence of an optical trap array subjected to an external drive. Sterically stabilized colloids with a hard-disk radius in the range of 2 to 5 μm can be captured by optical traps of radius 2 to 5 μm with an optical trapping force of 2.5 to 5.0 pN per trap, and experimentally arrays of up to 700 such traps can be produced with an intertrap spacing of 5 to 10 μm. Such a system can be mapped to our simulation by taking $l_0 = 10$ μm and $f_0 = 5$ pN. This gives $k = 0.5$ μN, a value consistent with what has been measured experimentally [52]. The driving force can be produced by a fluid flow, but this could induce additional hydrodynamic effects that are not included in our model. The sample can be tilted in order to produce a gravitational driving force; alternatively, in many optical trap systems the traps themselves can be moved, so an effective driving can be produced by translating the traps in order to induce different dynamical phases. Charged colloids with strong screening can be driven by an electric field.

III. VARIED DISK DENSITY

We first consider a fixed number of pinning sites $N_p = 1440$ with $F_p = 1.0$ as we vary the disk density from $\phi = 0.05$ to $\phi = 0.85$, giving a ratio of pinning sites to disks ranging from $N_p/N_d = 6.159$ to $N_p/N_d = 0.37$. With these parameters, a disk density of $\phi = 0.31$ corresponds to a ratio of $N_p/N_d = 1.0$. Figure 1(a) shows $\langle V_x \rangle$ versus F_D/F_p for different values of ϕ and Fig. 1(b) shows the corresponding $d\langle V_x \rangle/dF_D$ curves. In the inset of Fig. 1(b) we plot the depinning force F_c versus ϕ, indicating that F_c has a constant value of $F_c \approx F_p$ at low disk densities $N_p/N_d > 5.0$. Here F_c is the value of F_D at which disk motion first begins to occur. In this density range, almost every disk can be pinned directly by a pinning site, so collective interactions between the disks do not play an important role in the depinning process; instead, depinning

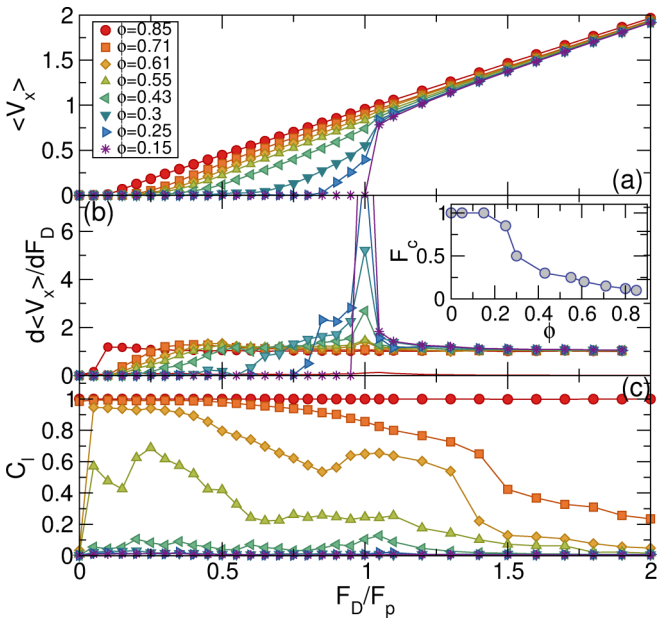

FIG. 1. (a) The average disk velocity $\langle V_x \rangle$ vs. driving force F_D/F_p for a system of harmonically interacting repulsive disks in a sample with $F_p = 1.0$ and $N_p = 1440$ at disk densities of $\phi = 0.85$ (red circles), 0.71 (orange squares), 0.61 (yellow diamonds), 0.55 (light green up triangles), 0.43 (medium green left triangles), 0.3 (dark green down triangles), 0.25 (blue right triangles), and 0.15 (purple stars). (b) The corresponding $d\langle V_x \rangle/dF_D$ vs. F_D/F_p curves showing a peak near $F_D/F_p = 1.0$. Inset: The depinning threshold F_c vs. ϕ, where $\phi \approx 0.3$ corresponds to a 1:1 ratio of disks to pinning sites. (c) The corresponding cluster size C_L vs. F_D/F_p.

occurs in the single particle limit and the depinning threshold is determined only by the value of F_p. For $N_p/N_d < 1.0$, some of the disks are not trapped by pinning sites, and these untrapped disks exert a force on the pinned disks, which lowers the depinning threshold, as shown in the inset of Fig. 1(a).

In Fig. 1(b), for $\phi \leqslant 0.55$ there is a pronounced peak in $d\langle V_x\rangle/dF_D$ near $F_D/F_p = 1.0$. This corresponds to the maximum pinning force from the substrate, so that for $F_D/F_p > 1.0$ all the disks are moving. For $N_p/N_d > 0.8$ or $\phi < 0.4$, a large fraction of the disks are located at pinning sites and the collision rate is low, so that most of the disks do not become mobile until $F_D/F_p > 1.0$, producing the jump in $\langle V_x\rangle$ at depinning at the lower fillings. For $N_p/N_d < 1.0$, there are excess disks that cannot be trapped directly by the pinning sites, and in principle these disks would be mobile for arbitrarily low F_D; however, they can still be indirectly pinned or blocked by disks that are located at the pinning sites, creating a local pile up or clogging configuration [39]. Since these interstitial disks exert forces on the disks located at the pinning sites, their presence reduces the depinning threshold by more than a factor of 2. For fillings $N_p/N_d = 1.0$ to 0.571, corresponding to $0.3 \leqslant \phi \leqslant 0.55$, some disks remain pinned until $F_D \geqslant F_p$, producing a weak peak in the $d\langle V_x\rangle/dF_D$ curves at $F_D/F_p = 1.0$. When ϕ is large enough, most of the disks are already moving for $F_D/F_p < 1.0$, and the peak feature is lost.

In Fig. 1(c) we plot the average value C_l of the size of the largest cluster normalized by the number of disks in the system as a function of F_D/F_p. To determine C_l, we use the cluster counting algorithm of Luding and Herrmann [53]. For $\phi < 0.43$, C_l is low and the largest clusters contain 10 or fewer disks. For $\phi \geqslant 0.43$, there is an increase in the cluster size at low drives due to a pile up effect in which unpinned disks accumulate behind pinned disks. For $\phi = 0.85$, the system forms a large cluster and $C_l = 1.0$ for all F_D. At $\phi = 0.55$, 0.61, and 0.71, there is a drop off in C_l for $F_D/F_p > 1.05$, 1.33, and 1.4, respectively, indicating a decrease in the cluster size. There is also a local maximum in C_l near $F_D/F_p = 1.0$ at $\phi = 0.61$.

A. Intermediate disk densities

In Fig. 1(c), for $\phi = 0.61$ there is an initial increase in C_l up to $C_l = 0.95$ at small but finite F_D/F_p due to the pile up effect. This is followed by a decrease in C_l to a local minimum near $F_D/F_p = 0.85$, and then by another increase to a local maximum in the range $0.85 < F_D/F_p < 1.4$, indicating a growth in the size of the largest cluster near $F_D/F_p = 1.0$. In Fig. 2(a) we plot the disk configurations for the $\phi = 0.61$ system at $F_D/F_p = 0.3$ where $C_l = 0.95$ showing large-scale clustering. An illustration of disk motion in the cluster state appears in Ref. [54]. Similar configurations appear at $F_D/F_p = 0.3$ for $0.43 < \phi < 0.85$. In Fig. 2(b), the corresponding structure factor $S(\mathbf{k}) = N_d^{-1}|\sum_i^{N_d} \exp(-i\mathbf{k}\cdot\mathbf{r}_i)|^2$ of the disk configuration has a ringlike feature indicative of a disordered system. As the drive is increased beyond the depinning transition, the clusters break apart and the disk density becomes homogeneous, as shown in Fig. 2(c) for $F_D/F_p = 0.7$, where a reduction in C_l has occurred. The corresponding structure factor in Fig. 2(d) still contains a

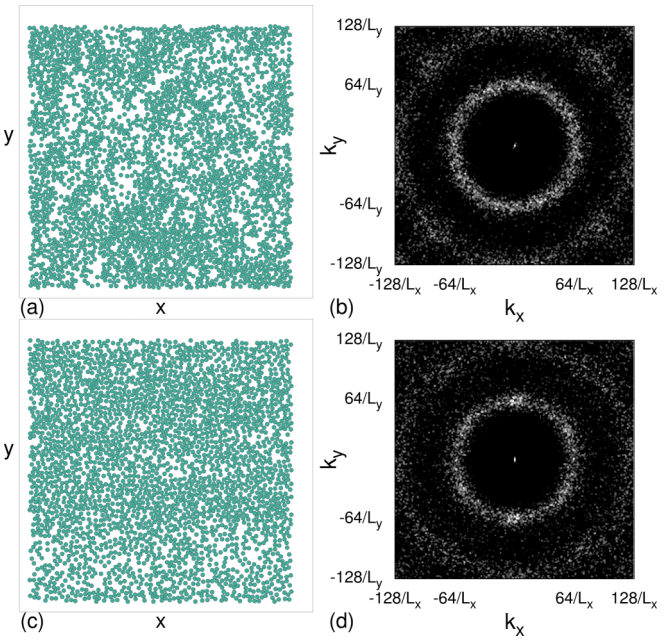

FIG. 2. (a) The disk positions (circles) for the system in Fig. 1 at $\phi = 0.61$ for $F_D/F_p = 0.3$, showing a clustering or pile up effect. (b) The corresponding structure factor $S(\mathbf{k})$ has a ringlike signature. (c) The driven homogeneous phase in the same system at $F_D/F_p = 0.7$. (d) The corresponding $S(\mathbf{k})$ plot from (c).

ringlike feature but has excess weight in two peaks along $k_x = 0$, indicating the formation of some chainlike structures due to the x-direction driving.

For $0.7 < F_D/F_p < 1.4$, the system forms a density phase separated state, as illustrated in Fig. 3(a) for $F_D/F_p = 1.05$. The motion of the disks in this state appears in [54]. Here there is a high-density region with $\phi \approx 0.85$ in which the disks have triangular ordering coexisting with a low-density region where the disks are disordered. The corresponding structure factor in Fig. 3(b) shows six peaks due to the triangular ordering within the dense phase. There is some smearing of the peaks along k_y due to the tendency of the crystallites in the dense phase to align with the driving direction. For $F_D/F_p > 1.4$, where C_l drops, the disks become more spread out and form 1D moving chains of the type shown in Fig. 3(c) at $F_D/F_p = 2.0$ and illustrated in a movie in [54]. The corresponding $S(\mathbf{k})$ in Fig. 3(d) has strong smectic ordering. In general, for $\phi \geqslant 0.43$ we find a phase separation in the vicinity of $F_D/F_p \approx 1$ similar to that shown in Fig. 3(a), where the extent of the dense region grows with increasing ϕ while the low-density regions become smaller.

B. Low disk density

For $\phi < 0.43$, the clumps that form near depinning are small, as illustrated in Fig. 4(a) at $\phi = 0.3$ and $F_D/F_p = 0.15$. The clumps are anisotropic and show some alignment along the y-direction, while the corresponding structure factor in Fig. 4(b) has a ringlike signature. At higher drives above depinning when some of the disks are moving, the disk density is more homogeneous, as shown in Fig. 4(c) at $F_D/F_p = 0.6$. The corresponding $S(\mathbf{k})$ plot in Fig. 4(d) has a more diffuse

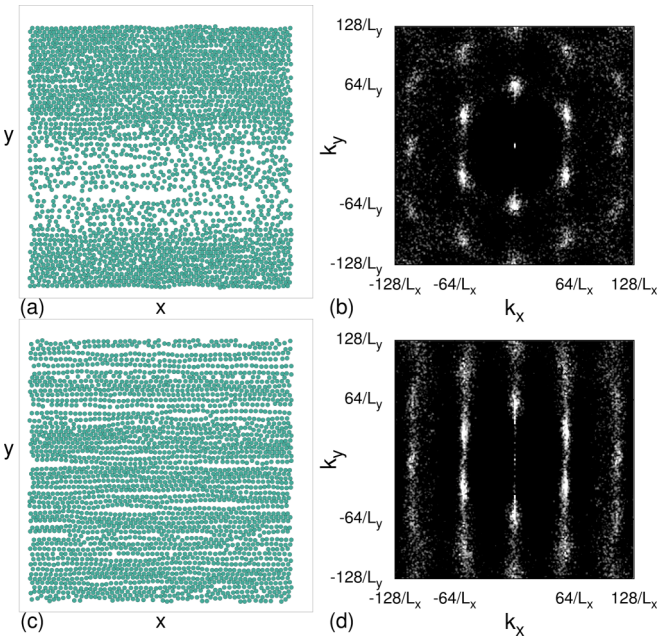

FIG. 3. (a) The disk positions (circles) for the system in Fig. 1 at $\phi = 0.61$ for $F_D/F_p = 1.05$, corresponding to the local maximum in C_l in Fig. 1(c). Here the system forms a density phase separated state. (b) The corresponding $S(\mathbf{k})$ plot contains sixfold peaks due to the triangular ordering in the dense phase. (c) The same system at $F_D/F_p = 2.0$ where a moving chainlike state forms. (d) The corresponding $S(\mathbf{k})$ shows smectic ordering.

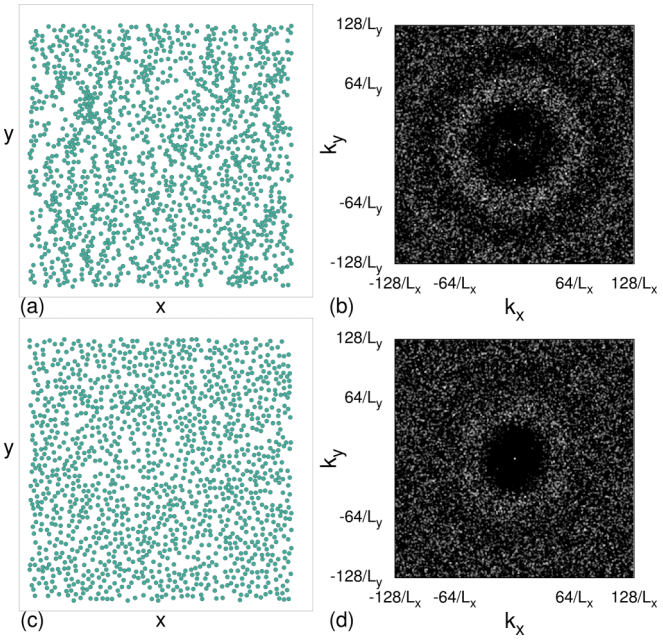

FIG. 4. (a) The disk positions (circles) for the system in Fig. 1 at $\phi = 0.3$ for $F_D/F_p = 0.15$, showing the formation of small clusters. (b) The corresponding $S(\mathbf{k})$ plot. (c) The same system at $F_D/F_p = 0.6$ in the moving phase where the disk density becomes homogeneous. (d) The corresponding $S(\mathbf{k})$ shows a diffuse or liquidlike pattern.

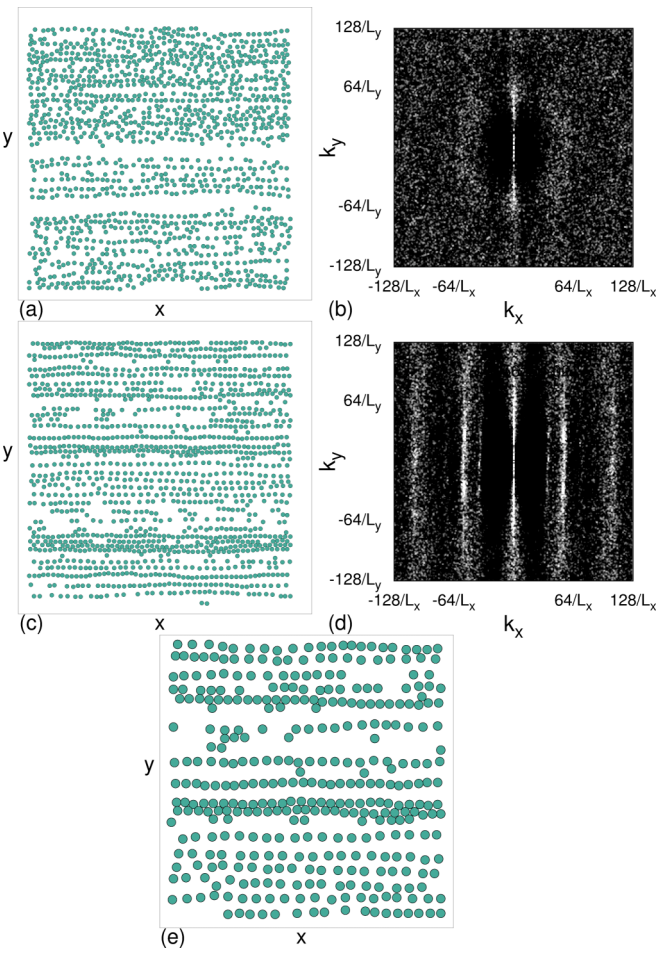

FIG. 5. (a) The disk positions (circles) for the system in Fig. 1 at $\phi = 0.3$ for $F_D/F_p = 1.05$, where the disks form chainlike patterns. (b) The corresponding $S(\mathbf{k})$ plot. (c) The same system at $F_D/F_p = 2.0$ in the moving phase where the disks form a series of chains or stripes. (d) The corresponding $S(\mathbf{k})$ has smectic ordering. (e) Blow up of disk positions from panel (c) showing formation of 1D chains.

structure. Near $F_D/F_p = 1.0$, most of the disks are in motion and form chainlike structures, as illustrated in Figs. 5(a) and 5(b) and in [54] for $F_D/F_p = 1.05$. The disk density is not uniform, with some chains closer together and others further apart; however, the denser regions are still too sparse to form sections of triangular lattice of the type that appear at $\phi = 0.61$ in Fig. 3(a). As F_D increases for the $\phi = 0.3$ sample, the moving chains of disks become better defined, as shown in Fig. 5(c) and in [54] at $F_D/F_p = 2.0$. The interchain spacing becomes small enough that the disks in neighboring chains are almost touching, and the corresponding structure factor in Fig. 5(d) shows strong smearing along the k_y direction.

These results indicate that even though ϕ is below the close-packed density of $\phi = 0.9$, different dynamic phases can arise and there can be transitions into states with smectic ordering, similar to the smectic states observed for driven superconducting vortices [9,20–22,24]. In general, the 1D channeling effect illustrated in Fig. 5(c) is much more pronounced in the disk system than in systems with longer-range interactions. The moving disks are unstable against the formation of chainlike structures due to a velocity collapse phenomenon. If one

moving disk slows down, the disk immediately behind it can run into it and cause it to speed up again, but once the two disks move beyond their steric interaction range, there are no particle-particle interactions to push them further apart, so the disks tend to pile up behind each other in the longitudinal direction. For $\phi = 0.85$, the system forms a dense cluster with polycrystalline triangular ordering, and for $F_D/F_p > 1.0$ the disks form a single triangular domain that is aligned with the driving direction.

We find two specific phenomena that differ from what is observed in systems of externally driven particles with longer-range interactions. These are: (1) a density phase separation, where high and low-density phases coexist as shown in Fig. 3(a), and (2) the formation of 1D chains as illustrated in Figs. 3(c) and 5(c). The density phase separation generally occurs in the range $0.9 < F_D/F_p < 1.2$, just above the drive at which all the disks become mobile, while the 1D chains appear for $F_D/F_p > 1.2$ when all the disks are rapidly flowing. In Fig. 5(e) we show a blow up of moving 1D chains from the system in Figs. 5(c) and 5(d), indicating that the chains form in the longitudinal direction, and that in this direction the disks are almost touching to give a density along the length of the chain close to $\phi = 0.9$. Although clustering has been observed in active matter systems [44–46], such 1D chaining does not occur for active disk systems, and results from a combination of the x direction driving force and the highly anisotropic fluctuations of the moving disks.

C. Transverse diffusion and topological order

We can characterize the different phases by measuring the particle displacements in the direction transverse to the applied drive, $\langle \delta y^2 \rangle = N_d^{-1} \sum_{i=1}^{N_d} (y_i(t) - y_i(t_0))^2$, for varied F_D/F_p. In general we find $\langle \delta y^2 \rangle \propto t^\alpha$ at long times. In the disordered homogeneous density regimes, $\alpha = 1.0$, indicative of diffusive behavior, while $\alpha < 1.0$ just above depinning and in the moving chain state. In Fig. 6 we plot the value of $\langle \delta y^2 \rangle$ obtained at a fixed time of 5×10^6 simulation time steps versus F_D/F_p along with the corresponding value of α for the system in Fig. 1 at $\phi = 0.25$, 0.3, 0.43, 0.55, 0.61, and 0.71. For $\phi = 0.25$ and $\phi = 0.3$ in Figs. 6(a) and 6(b), there is a peak in $\langle \delta y^2 \rangle$ near $F_D/F_p = 1.0$, where $\alpha \approx 1.0$, indicating diffusive behavior. The maximum amount of transverse diffusion falls at the same value of F_D/F_p as the peak in $d\langle V_x \rangle / dF_D$ shown in Fig. 1(b). At low drives where the system forms a clogged state, the transverse diffusion is suppressed. At higher drives where the disks form 1D channels, the diffusion in the direction transverse to the drive is strongly suppressed and $\alpha \to 0$, indicating that the 1D channels are frozen in the transverse direction.

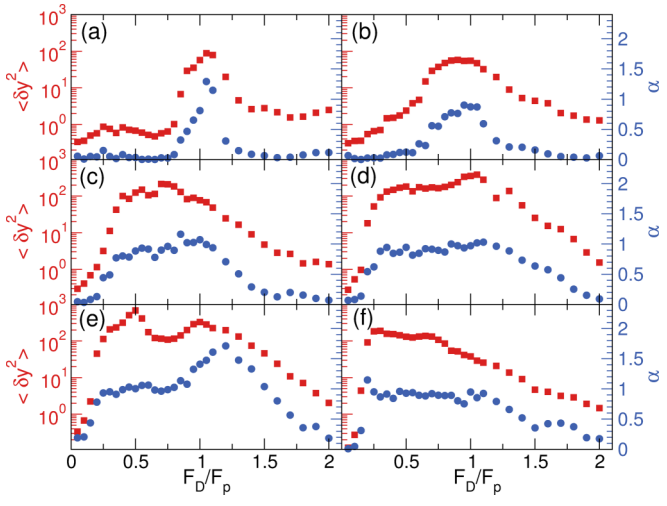

FIG. 6. The transverse displacements $\langle \delta y^2 \rangle$ obtained after 4×10^6 simulation time steps (red squares) and the diffusive exponent α (blue circles) vs. F_D/F_p for the system in Fig. 1 at $\phi =$ (a) 0.25, (b) 0.3, (c) 0.43, (d) 0.55, (e) 0.61, and (f) 0.71.

For $\phi = 0.43$, 0.55, and 0.61 in Figs. 6(c)–6(e), $\langle \delta y^2 \rangle$ has a double peak feature. The first peak corresponds to the onset of the homogeneous moving phase, while the second peak occurs when the system starts to undergo phase separation. For $\phi = 0.61$, where the strongest phase separation is observed, there is even a region of drive for which $\langle \delta y^2 \rangle$ exhibits superdiffusive behavior with $\alpha > 1.0$. At longer times the behavior transitions to regular diffusion. For higher drives, both $\langle \delta y^2 \rangle$ and α decrease with increasing drive as the system forms a moving chain state. For $\phi = 0.71$ in Fig. 6(f), the double peak feature begins to disappear. Numerical studies of vortices in type-II superconductors [24,55] show that the vortices exhibit strong transverse diffusion above the depinning transition, while at higher drives where a moving smectic state appears, the transverse diffusion is strongly suppressed and the system freezes in the transverse direction. The vortex system typically has only a single peak in $\langle \delta y^2 \rangle$ rather than the double peaks we observe here. The regime of superdiffusive behavior for $\phi = 0.61$ arises due to collective transverse motion of the disks in the dense phase.

Another measure often used to characterize interacting particles driven over disorder is the fraction P_6 of sixfold coordinated particles. Here $P_6 = N_d^{-1} \sum_i^{N_d} \delta(z_i - 6)$, where z_i is the coordination number of disk i obtained from a Voronoi tessellation. In the case of superconducting vortices in the absence of pinning, the ground state is a triangular lattice with $P_6 = 1.0$, while when strong disorder is present, the pinned state is disordered and contains numerous topological defects so that $P_6 < 1.0$. At high drives, where the effect of pinning is reduced, the system can dynamically reorder into a moving triangular lattice with $P_6 = 1.0$ or into a moving smectic where some topological defects persist that are aligned with the direction of drive, giving $P_6 \lesssim 1$ [3,4,17,20–22,24].

In Fig. 7 we plot P_6 versus F_D/F_p for the system in Fig. 1 at $\phi = 0.25$, 0.3, 0.43, 0.61, 0.71, and 0.85. Although there are several similarities to the behavior of P_6 observed for superconducting vortices, there are a number of notable differences. For $\phi = 0.25$ and $\phi = 0.3$ in Figs. 7(a) and 7(b), there is an increase in P_6 above $F_D/F_p = 1.0$ which corresponds to the formation of the moving chain state illustrated in Fig. 5(a), followed by a saturation of P_6 at higher drives to $P_6 = 0.55$. This is in marked contrast to the behavior observed in the vortex system, where P_6 saturates to a value much closer to $P_6 = 1.0$ due to the longer-range particle-particle repulsion which favors the formation of a triangular vortex lattice down to quite low vortex densities. At $\phi = 0.43$ in Fig. 7(c), P_6 shows a similar trend as in the

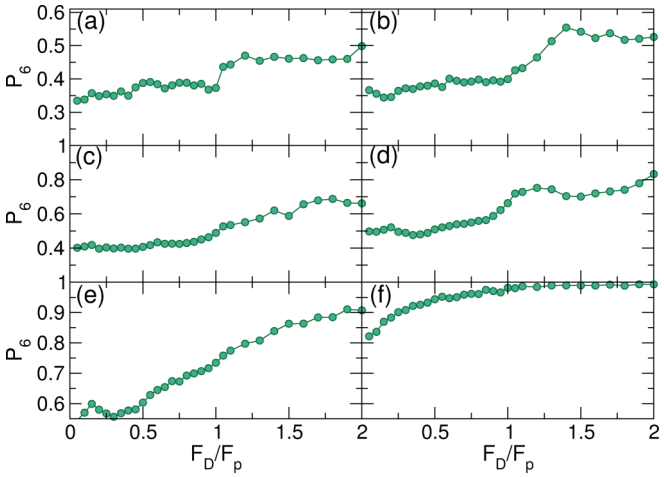

FIG. 7. The fraction P_6 of sixfold coordinated disks vs. F_D/F_p for the system in Fig. 1 for $\phi =$ (a) 0.25, (b) 0.3, (c) 0.43, (d) 0.61, (e) 0.71, and (f) 0.85. For $\phi = 0.61$ in panel (d), the local maximum in P_6 near $F_D = 1.0$ is correlated with the formation of the phase separated state shown in Fig. 3(a).

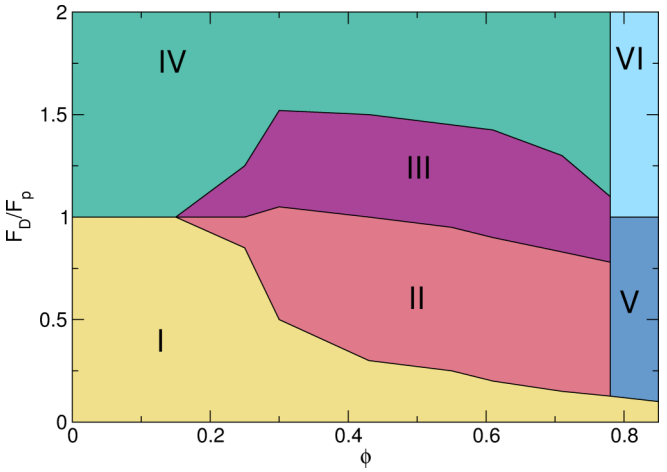

FIG. 8. Schematic phase diagram as a function of F_D/F_p vs. ϕ for the system in Fig. 1. I: Pinned or clogged state. II: Homogeneous plastic flow. III: Density phase separated state. IV: Moving smectic or moving chain state. V: Moving polycrystalline state. VI: Moving crystal state.

systems with lower disk densities; however, P_6 saturates to a higher value of $P_6 = 0.68$. In Fig. 7(d) at $\phi = 0.61$, there is a local maximum in P_6 for $0.9 < F_D/F_p < 1.4$ that coincides with the density phase separated regime. The disks in the dense phase have mostly triangular ordering, as shown in Figs. 3(a) and 3(b). For higher drives of $F_D/F_p > 1.4$, where the disks become more spread out, P_6 drops again. At $\phi = 0.71$ in Fig. 7(e), for low drives $P_6 \approx 0.55$, and then P_6 gradually increases with increasing drive up to a value of $P_6 = 0.9$, indicating that most of the sample has developed triangular ordering. Finally, for $\phi = 0.85$ in Fig. 7(f), at the lowest drives the system forms a polycrystalline solid containing a small number of defects, so that the initial value of $P_6 \approx 0.81$, while as F_D increases, the polycrystal anneals into a single domain crystal that is aligned in the direction of drive, with $P_6 = 0.99$, indicating almost complete triangular ordering.

For $0.3 < \phi < 0.85$, the P_6 curves in Fig. 7 show a small peak near $F_D/F_p = 0.2$ due to the pile up or clustering effect. Within the clusters the local density $\phi_{\rm loc}$ is $\phi_{\rm loc} \approx 0.85$, producing increased sixfold ordering and a corresponding increase in P_6. Once the drive is large enough to break apart these clusters, there is a drop in P_6 as the system enters the homogeneous moving phase.

D. Dynamic phase diagram

From the features in the velocity-force curves, P_6, $\langle \delta y^2 \rangle$, and the disk configurations, we can construct a schematic phase diagram of the evolution of the different phases, as shown in Fig. 8. Phase I corresponds to the pinned or clogged state, phase II is homogeneous disordered plastic flow, phase III is the density phase separated state, phase IV is the moving smectic or moving chain state, phase V is the moving polycrystalline state, and phase VI is the moving single domain crystal state.

Many of the features in the phase diagram can be understood with force balance arguments. The depinning line separating phase I from phase IV for $\phi < 0.2$ falls at the constant value of $F_D/F_p = 1$. At these low disk densities the disks are pinned individually, so the depinning threshold is determined only by the value of F_p. For $\phi > 0.2$, not all of the disks are directly captured by pinning sites; instead, some disks are unable to find an empty pinning site and move through the system as interstitials, pinned only through their interaction with directly pinned disks. The interstitials can flow plastically, so phase II exists only when interstitials are present. Interstitials emerge once a percolating fraction $p_f \sim 0.67$ of the pinning sites are filled, so if we write $\phi_{\rm equiv} = 0.314$ as the density of disks that we would have if every pinning site were filled with exactly one disk, we expect the onset of phase II flow to occur for $\phi \gtrsim p_f \phi_{\rm equiv} = 0.21$. For $\phi > 0.2$, due to the pairwise disk interactions the depinning threshold gradually becomes dominated by the driving force at which an unpinned disk can depin a pinned disk with which it is in contact, reducing the depinning threshold from $F_c = F_p$ to $F_c = F_p/2$. In Fig. 8, the depinning line separating phases I and II gradually decreases from $F_D/F_p = 1$ at $\phi = 0.2$ to $F_D/F_p = 0.5$ at $\phi = 0.3$. As ϕ increases further, three or more disks can come into contact and the depinning force falls off as $F_c = F_p/(N_{\rm avg} + 1)$ where $N_{\rm avg}$ is the average number of unpinned disks in force contact with a pinned disk. Since $N_{\rm avg}$ increases with disk density we expect $F_c \sim F_p/\phi$, consistent with the decrease in the depinning line marking the end of phase I for $\phi > 0.3$ in Fig. 8.

Phase II in Fig. 8 consists of a combination of pinned and moving disks. Since all of the disks depin for $F_D/F_p \geqslant 1.0$, the upper boundary of phase II should be close to $F_D/F_p = 1$, as we observe. Similarly to the depinning line, the upper boundary of phase II gradually decreases with increasing ϕ as multiple disk interactions, which tend to depin the pinned disks, become more important. For $\phi \gtrsim 0.77$ the system is so dense that the depinning becomes elastic, as observed in earlier studies of depinning for binary disk systems, so that phase II disappears and is replaced by phase V, which again extends up to a maximum drive of $F_D/F_p = 1$. The $\phi \approx 0.77$

line separating the high-density phases V and VI from the lower-density phases is a type of random close packing (RCP), but it falls below the clean system RCP value of $\phi = 0.82$ [56,57] due to the presence of the quenched disorder.

Phase III, the phase separated state, in Fig. 8 occurs when two conditions are met: (1) all the disks are moving, and (2) the dynamical fluctuations are strong enough that the moving disks have a component of their root-mean square (RMS) motion in the direction transverse to the drive that is ballistic over a sufficiently long time interval to permit noticeable transverse grain motion to occur. Phase III only occurs for $\phi > 0.2$, in agreement with previous work [19], and consistent with the observation in active matter that cluster formation occurs only for sufficiently high density and activity. For $F_D/F_p < 1.0$ there are still pinned disks present that can interfere with the phase separation and make the density more uniform, so the lower boundary of phase III falls near $F_D/F_p \approx 1.0$. The transverse RMS motion of the disks decreases with increasing F_D since the magnitude of the fluctuations δy induced by the pinning sites diminishes as the disks travel faster, $\delta y \propto 1/F_D$, similar to the effective temperature found in superconducting vortex systems. Once these transverse fluctuations become small enough, the clustering is lost. This has similarities to the loss of clustering in active matter systems as the run length is reduced [45,46] or the active diffusion is reduced [58,59], but the origin of the fluctuations in the disk and the active matter systems is quite different.

When the drive is high enough and the transverse displacements $\langle \delta y^2 \rangle$ are smaller than the longitudinal fluctuations, the system enters the moving chain state marked phase IV in Fig. 8. This phase is analogous to the moving smectic state found for vortices driven over random disorder [19–22,24]; however, unlike the vortices, the disks can form chains that have an almost close-packed density of $\phi = 0.9$ along their length while still experiencing zero overlap energy as long as the disks are not touching. In contrast, for a system with longer-range interactions of $1/r$, $e^{-\kappa r}/r$, or Bessel function form, due to the energy divergence at small r such extreme chaining would be very energetically costly and hence would be unstable. As F_D further increases, the longitudinal fluctuations δx also decrease in magnitude; however, once the system has entered the chain state, the chains can persist up to arbitrarily high drives. At densities $\phi > 0.77$, above the RCP transition to elastic pinning, Fig. 8 indicates that for high drives the system forms the moving solid state marked phase VI.

To highlight the role of the effective shaking temperature or activity in inducing dynamic phase changes, in Fig. 9 we plot a schematic of A, the amplitude of the effective shaking temperature or the effective activity, versus F_D/F_p at $\phi = 0.3$. The I-II transition occurs when the force $F_D^{\rm net}$ acting on all n interstitial disks in contact with a pinned disk as well as on the pinned disk itself exceeds the pinning force F_p. At $\phi = 0.3$, as shown in Fig. 9, there is an average of $n = 1$ interstitial disk in contact with each pinned disk, so $F_D^{\rm net} = (n+1)F_D = 2F_D$ and depinning occurs at $F_D/F_p = 0.5$; in contrast, for $\phi < 0.2$, $n = 0$ and depinning occurs at $F_D/F_p = 1.0$. The activity A in the pinned phase I is $A = 0$. For $0.5 < F_D/F_p < 1.0$, the system is in phase II and contains both pinned and moving disks. In this case the shaking activity is bimodal and the fluctuations are strongly non-Gaussian, so A is not well defined

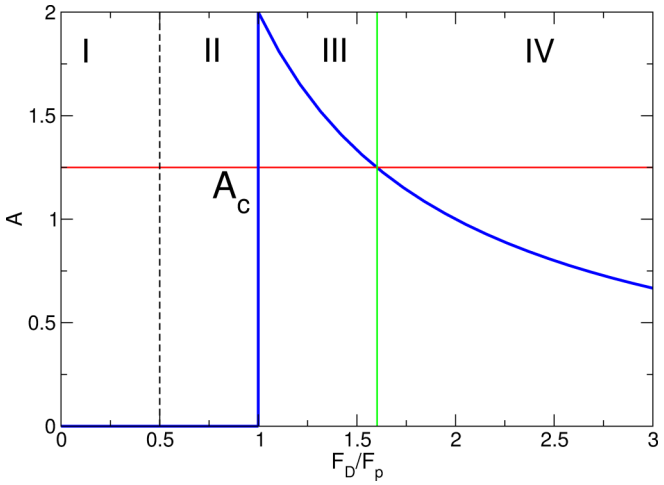

FIG. 9. Schematic plot of the effective shaking temperature or activity A vs. F_D/F_p for a sample with $\phi = 0.3$. The vertical dashed black line at $F_D/F_p = 0.5$ separates the pinned phase (I) from homogeneous plastic flow (II). At $F_D/F_p = 1.0$ all the particles begin to move, producing an effective shaking temperature or activity with an amplitude A that decreases as $1/F_D$. There is a critical shaking activity, A_c (horizontal red line), above which clustering can begin to occur, so that a phase separated state (III) appears above $F_D/F_p = 1.0$. Phase III disappears above the value of F_D/F_p marked by a vertical solid green line, which is determined by the point at which A drops below A_c. At high drives where $A < A_c$, Phase IV, the moving smectic state, appears as the externally applied driving force begins to dominate the behavior of the system and the effective shaking temperature becomes unimportant.

and we indicate its value as $A = 0$. For $F_d/F_p > 1.0$ all the particles are moving, so A is well defined and has its highest value at $F_D/F_p = 1.0$ before decreasing according to $A \sim 1/F_D$. We can define a disk density-dependent critical activity level, A_c, needed for clustering to occur. As long as $A > A_c$, the system remains in phase III, but when A drops below A_c, clustering is lost and the system transitions into phase IV.

IV. VARIED PINNING DENSITY

We next consider the case of a fixed disk density of $\phi = 0.55$, corresponding to $N_d = 2500$, and vary the number of pinning sites to give a ratio of N_p/N_d ranging from $N_p/N_d = 0$ to $N_p/N_d = 0.576$. In Figs. 10(a) and 10(b) we show $\langle V_x \rangle$ and $d\langle V_x \rangle/dF_D$ versus F_D/F_p for a sample with $F_p = 1.0$. There is one peak in $d\langle V_x \rangle/dF_D$ near $F_D/F_p = 1.0$, the drive above which all of the disks are moving, and a second peak near $F_D/F_p = 0.5$, the drive at which the clogged state breaks apart. We observe a similar set of dynamical phases as those described in Sec. III, but find that the density phase separated state is more prominent at lower pinning density, as shown in the plots of C_l versus F_D/F_p in Fig. 11 for $N_p/N_d = 0.072$, 0.216, 0.288, and 0.432. In particular, $N_p/N_d = 0.216$ in Fig. 11(b) and $N_p/N_d = 0.288$ in Fig. 11(c) exhibit strong peak features associated with the density phase separated state. The double peak feature in the $d\langle V_x \rangle/dF_D$ curves is generally absent for 2D studies of particles with longer-range repulsion driven over disorder, where typically only one peak is observed, and is thus a unique feature of the 2D disk system. In

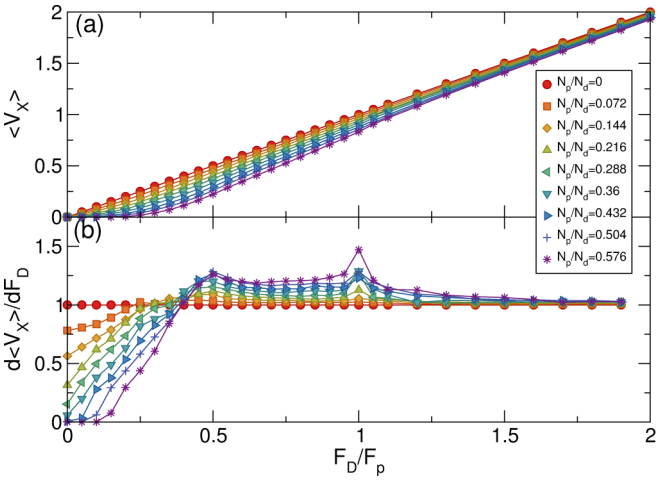

FIG. 10. (a) $\langle V_x \rangle$ vs. F_D/F_p at $\phi = 0.55$ and $F_p = 1.0$ for $N_p/N_d = 0.0$, 0.072, 0.144, 0.216, 0.288, 0.36, 0.432, 0.504, and 0.576, from top to bottom. (b) The corresponding $d\langle V_x \rangle/dF_D$ vs. F_D/F_p curves showing peaks near $F_D/F_p = 0.5$ and $F_D/F_p = 1.0$.

addition, for particles with longer-range interactions, measures of P_6 and hence C_l generally show only monotonic behavior above depinning, in contrast to the disk system, which shows a clear nonmonotonic behavior with a second peak near $F_D/F_p = 1.0$.

To show more clearly the evolution of the cluster state, in Fig. 12 we illustrate the disk positions for the system at $N_p/N_d = 0.288$ for increasing F_D. The letters a through f in Fig. 11(c) indicate the values of F_D/F_p that match these images. In Fig. 12(a) at $F_D/F_p = 0.05$, where $C_l = 0.85$, the system forms a clogged state. Within the cluster regions, which are colored red, the disk density is close to $\phi = 0.85$, and these clusters are separated by low-density regions of disks. As the drive increases, the large cluster becomes more spread out, as shown in Fig. 12(b) for $F_D/F_p = 0.3$, where C_l drops to

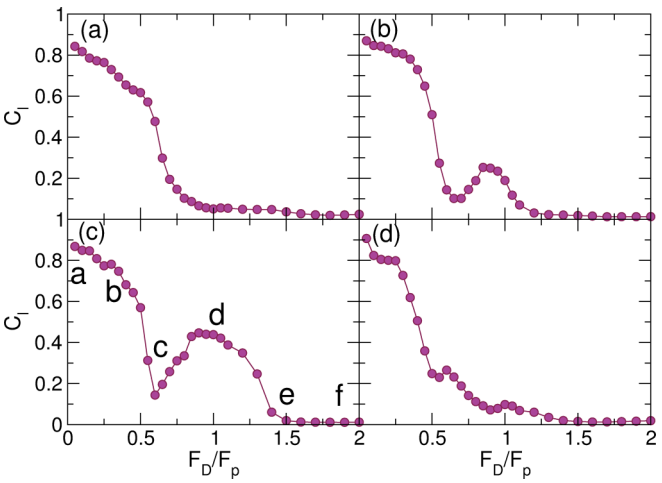

FIG. 11. Cluster size C_l vs. F_D/F_p for the system in Fig. 10 at $N_p/N_d =$ (a) 0.072, (b) 0.216, (c) 0.288, and (d) 0.432. The local peaks in (b) and (c) correspond to the formation of a density phase separated state. In panel (c) the lettering indicates the F_D/F_p values represented in the real space images in Fig. 12.

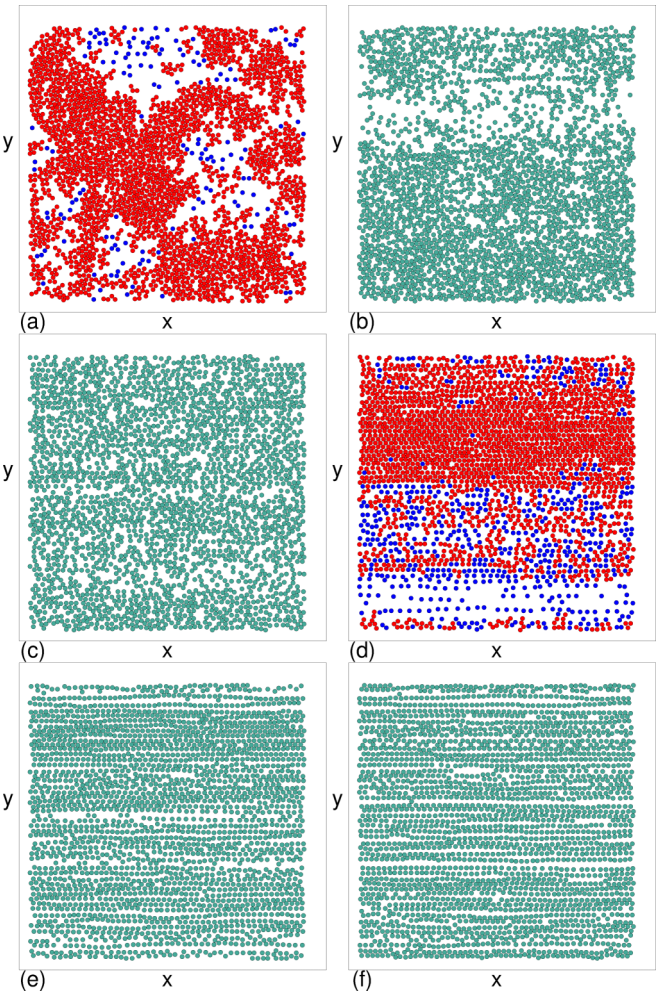

FIG. 12. The disk positions for the system in Figs. 10 and 11 at $N_p/N_d = 0.288$ for drive values marked with letters in Fig. 11(c). In panels (a) and (d), red disks are part of clusters containing three or more disks, while blue disks are isolated or in a cluster containing only two disks. (a) The pinned cluster state at $F_D/F_p = 0.05$. (b) At $F_D/F_p = 0.3$ the moving disks form more spread out clusters. (c) At $F_D/F_p = 0.6$, corresponding to the local minimum of C_l in Fig. 11(c), a homogeneous disordered state forms. (d) At $F_D/F_p = 1.05$, corresponding to the peak in C_l in Fig. 11(c), a density phase separated state forms. At (e) $F_D/F_p = 1.5$ and (f) $F_D/F_p = 2.0$, the disks are in a moving chain state.

$C_l = 0.78$. At $F_D/F_p = 0.6$ in Fig. 12(c), which corresponds to a local minimum in C_l in Fig. 11(c), the disks are completely spread out and form a homogeneous disordered phase. In Fig. 12(d) at $F_D/F_p = 1.05$, which corresponds to a local maximum in C_l in Fig. 11(c), a density phase separated state appears. Disks that are in a cluster containing at least three disks are colored red in order to more clearly highlight the dense region, within which the disks have developed triangular ordering. As the drive is further increased, the disks spread apart in the direction transverse to the drive to form the moving chain state illustrated in Figs. 12(e) and 12(f) at $F_D/F_p = 1.5$ and $F_D/F_p = 2.0$, respectively, which also coincides with a reduction of C_l in Fig. 11(c). For $N_p/N_d = 0.55$ and above,

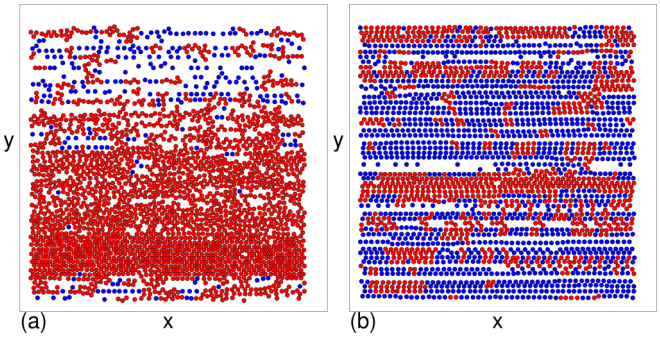

FIG. 13. The disk positions for a system with $\phi = 0.55$ at $N_p/N_d = 0.072$, where there is no peak in C_l in Fig. 11(a). Red disks are part of clusters containing three or more disks, while blue disks are isolated or in a cluster containing only two disks. (a) A density phase separated state at $F_D/F_p = 0.3$. (b) A moving chain state forms at higher drives, shown here at $F_D/F_p = 1.5$.

the density phase separated state becomes less well defined, as indicated in Fig. 11(d) at $N_p/N_d = 0.432$.

In Fig. 11(a) at $N_p/N_d = 0.072$, although C_l does not show a peak near $F_D/F_p = 1.0$, there is still a pronounced density phase separated state; however, this phase has shifted to lower F_D/F_p. Since the low-density clogged state transitions directly into the flowing density phase separated state, there is no dip in C_l. The density phase separated state breaks apart at lower values of F_D/F_p compared to samples with higher values of N_p/N_d. In Fig. 13(a) we show the disk configurations at $N_p/N_d = 0.072$ and $F_D/F_p = 0.3$ where a density phase separated state appears, while in Fig. 13(b) we illustrate the moving chain phase that forms at $F_D/F_p = 1.5$ in the same system. From the images we can construct a schematic phase diagram for the $\phi = 0.55$ sample as a function of F_D/F_p versus N_p/N_d, as shown in Fig. 14(a), which highlights the extents of regions I through IV. Here, the widths of regions I and II grow with increasing N_p/N_d, while region III reaches its largest extent near $N_p/N_d = 0.3$. We note that for $N_p/N_d = 0$, the system forms a moving disordered state for all $F_D > 0$.

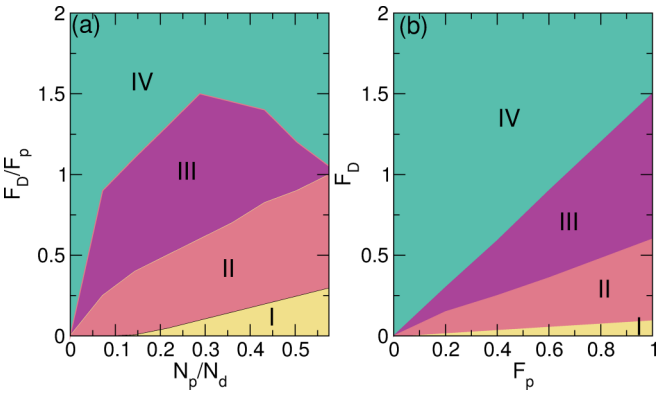

FIG. 14. (a) Schematic phase diagram as a function of F_D/F_p vs. N_p/N_d for the system in Fig. 10 at fixed $\phi = 0.55$. I: Pinned or clogged state. II: Homogeneous plastic flow. III: Density phase separated state. IV: Moving smectic or moving chain state. (b) Phase diagram for the same system at $\phi = 0.55$ and $N_p/N_d = 0.288$ as a function of F_D vs. F_p.

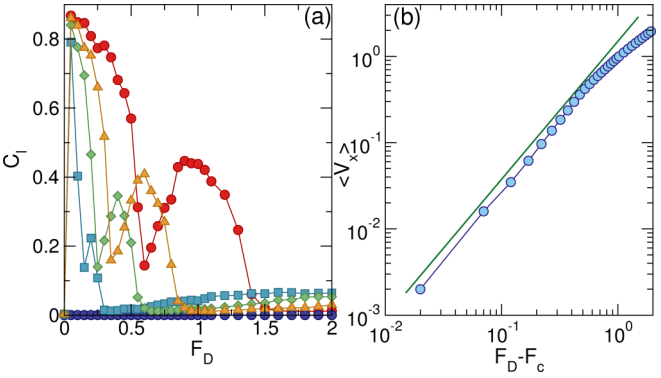

FIG. 15. (a) The cluster size C_l vs. F_D for samples with $\phi = 0.55$ and $N_p/N_d = 0.288$ at $F_p = 0.0$ (blue circles), 0.2 (blue squares), 0.4 (green diamonds), 0.6 (orange triangles), and 1.0 (red circles). (b) $\langle V_x \rangle$ vs. $F_D - F_c$ for the velocity-force curve obtained at $\phi = 0.55$ and $N_p/N_D = 0.576$. The solid line is a power law fit with an exponent of $\beta = 1.6$.

In the dynamic phase diagram of Fig. 14(a), the depinning transition marking the upper bound of phase I increases linearly with increasing N_p, a behavior similar to that observed in other systems, such as superconducting vortices, that exhibit plastic depinning [1]. The upper boundary of phase III varies nonmonotonically with N_p due to the behavior of the fluctuations. Phase III arises due to the transverse fluctuations produced by a combination of interactions with the pinning sites and disk-disk collisions. When N_p is small, there are not enough pinning sites to create strong nonequilibrium fluctuations, so the extent of phase III decreases with decreasing N_p. At high N_p, the situation is similar to that in the phase diagram of Fig. 8 at high ϕ, where fluctuations in the disk motion are larger in the longitudinal or x direction than in the transverse or y direction, and as a result chain-like structures are destabilized and the width of phase III decreases with increasing N_p.

We have considered varying F_p while holding ϕ and N_p/N_d fixed, and find that the same general phases appear. In Fig. 14(b), the upper boundary of phase I increases linearly with increasing F_p, as expected for a depinning transition. The line separating phases II and III marks the point at which all of the disks are moving, and this line also increases linearly with F_p. The line separating phases III and IV appears at the point when the transverse fluctuations become too small to permit density phase separation to occur, and since the fluctuations are affected by the pinning strength, this line also increases linearly with F_p. In Fig. 15(a) we plot C_l versus F_D in a sample with $\phi = 0.55$ and $N_p/N_d = 0.288$ for $F_p = 0.0$, 0.2, 0.4, 0.6, and 1.0 to show the evolution of the second peak, which both increases in width and shifts to higher values of F_D as F_p increases.

For depinning in systems with longer-range interactions, such as superconducting vortices, colloidal particles, and electron crystals, scaling near the depinning threshold is observed in the velocity-force curves, which have the form $V \propto (F_D - F_c)^{-\beta}$. In plastic depinning, where particles exchange neighbors as they move, $\beta > 1.0$, while for elastic depinning, in which the particles maintain the same neighbors as they move, $\beta < 1.0$ [1]. In systems with long-range Coulomb

interactions [8] and screened Coulomb interactions [12,60], plastic depinning is associated with exponents of $\beta \approx 1.65$ and $\beta \approx 2.0$, respectively. More recently, simulations of depinning of superconducting vortices with a Bessel function vortex-vortex interaction give $\beta = 1.3$ [61]. Due to the observed variations in these exponents, it is not clear that existing simulations of plastic depinning are large enough to accurately obtain the true scaling since it is expected that a critical phenomenon would be associated with a unique exponent.

It is interesting to ask whether similar scaling of the velocity-force curves occurs in the disk system. In Fig. 15(b) we plot $\langle V_x \rangle$ versus $F_D - F_c$ on a log-log scale for a sample with $\phi = 0.55$ at $N_p/N_D = 0.576$. The solid line indicates a scaling fit with $\beta = 1.6$. At higher drives, well above depinning, the slope of the velocity-force curve becomes linear, as expected since the effectiveness of the pinning is lost in this regime. In general, we find that for $N_p/N_d > 0.288$, the velocity-force curves can be fit to a power law with $1.4 < \beta < 1.7$. The variation in the exponents we obtain is a result of the limited size of our simulation, but our values are within the range of those reported for plastic depinning of systems with longer-range interactions [8,12,60]. It remains an open question whether plastic depinning for systems with short-range interactions falls in the same universality class as plastic depinning for systems with long-range interactions. For $N_p/N_d < 0.288$, the depinning threshold $F_c = 0$ since there are few enough pinning sites that some disks can pass completely through the system without being trapped directly by pinning or indirectly by becoming lodged behind pinned disks.

V. DISCUSSION

The dynamic density phase separation we find has not been observed in studies of superconducting vortices or colloids driven over random disorder. As noted previously, under certain conditions such as low flux density or very small penetration length, superconducting vortices could behave like a hard-disk system and exhibit density phase separation or the formation of 1D flowing chains. Observation of such effects would require the use of weak pinning samples that provide access to the flux flow regime at low fields. There have been examples of clump-like vortex states observed at low fields in certain materials; however, these clumps may be the result of competing attractive and repulsive interactions between the vortices [51], rather than from reaching an effective hard-disk interaction limit. There have been some numerical studies of vortex avalanches in which the vortex-vortex repulsion was modeled as as harmonic repulsion [62]; however, these studies were performed in a 1D system, which is a very different limit from the system we consider. Numerical studies of vortices moving through periodic substrate arrays showed that under certain conditions the system can form vortex density or soliton waves [63]; however, these studies are again in a very different regime from that which we consider. There has also been work showing that phase separation into high-density regions as well as stripe ordering occurs for particles driven over random disorder when the pairwise interactions between particles include both a repulsive and an attractive term [64,65]; however, in the disk system we consider here, the disk-disk interaction is purely repulsive.

The phase separation we observe has similarities to the active matter clustering found in simulations of hard disks undergoing active Brownian motion or run-and-tumble-type dynamics. In the active matter systems, when the activity is high enough, the particles phase separate into a dense solidlike region and a low-density fluid [43–46] due to a combination of the nonequilibrium nature of the fluctuations and the fact that the mobility of the particles is dependent on the local particle density [44]. In the driven disk system, velocity fluctuations transverse to the driving direction are generally largest when there is a coexistence of disks being pinned or slowed down by the pinning along with faster moving unpinned disks. When the disks collide with each other, they generate velocity fluctuations that have a ballistic component in the transverse direction, similar to the motion of active particles. This also produces time intervals in the transverse diffusion that exhibit superdiffusive behavior similar to that found in active matter systems [46]. Additionally, the disks have a reduced mobility when the disk density increases. When the drive is large enough, both the speed differential of the disks and the velocity fluctuations transverse to the drive are lost, and since these effects are necessary to produce the clustering and the density phase separation, the clustering and density phase separation also disappear. The same effects could arise in systems with longer-range interactions; however, the large energy cost of high-density regions would suppress the density phase separation we observe for the short-range repulsive disks. Experimentally, the dynamic phase separation could be observed using colloids, emulsions, or micelles that have only steric interactions moving over random substrates. Experiments with quasi-2D granular systems could include grains flowing over a rough landscape under the influence of gravity or shaking; however, in this case, inertial and intergrain frictional effects would also need to be taken into account. In our work we focus on the case of monodisperse disks, so that the system forms triangular ordering in the dense phase; however, we have also considered a case for bidisperse disks with a radius ratio of 1 : 1.4 and find the same features, where the phase separated state is shifted to a somewhat lower density, suggesting that the dense phase separated regions are in fact jammed since it is well known that jamming occurs for lower densities in bidisperse disks than for monodisperse disks [38].

VI. SUMMARY

We have numerically examined the dynamical phases for monodisperse repulsive disks driven over random disorder. Despite the simplicity of this system, we observe a rich variety of distinct dynamics, many of which have significant differences from the dynamic phases observed for other systems of collectively interacting particles with longer-range repulsion, such as vortices in type-II superconductors and colloids with Yukawa interactions. The phases we find include a heterogeneous clogged state where the disks form local immobile clumps, a homogeneous disordered plastic flow state, a moving density phase separated state where the system forms a dense region with mostly triangular ordering coexisting with a low-density disordered phase, and a stripe or

chainlike state at higher drives. The density phase separation occurs due to the density dependent mobility of the disks and the short-range nature of their interaction with each other, which permits the disks to pack closely together with little overlap energy. In contrast, in systems with longer-range repulsion, density phase separated states are prevented from forming since more homogeneous states have a much lower particle-particle interaction energy. The chain formation can occur in the disk system since the disks can approach almost within a radius of each other without paying an overlap energy cost, whereas in systems with longer-range interactions, such strongly anisotropic structures would have a very high energy cost. From the features in the transverse diffusion, structure factor, and velocity-force curves, we map the evolution of the different phases as a function of disk density, pinning site density, and pinning force. Our results suggest that the dynamic density phase separation and the chainlike state should be general features in systems with short-range steric interactions driven over random disorder. These effects could be observed experimentally using sterically interacting colloids, emulsions, micelles, and even superconducting vortices at low fields moving over random disorder.

ACKNOWLEDGMENTS

This work was carried out under the auspices of the NNSA of the U.S. DoE at LANL under Contract No. DE-AC52-06NA25396.

[1] C. Reichhardt and C. J. Olson Reichhardt, Depinning and nonequilibrium dynamic phases of particle assemblies driven over random and ordered substrates: A review, Rep. Prog. Phys. **80**, 026501 (2017).

[2] H. J. Jensen, A. Brass, Y. Brechet, and A. J. Berlinsky, Current-voltage characteristics in a two-dimensional model for flux flow in type-II superconductors, Phys. Rev. B **38**, 9235 (1988).

[3] S. Bhattacharya and M. J. Higgins, Dynamics of a Disordered Flux Line Lattice, Phys. Rev. Lett. **70**, 2617 (1993).

[4] M. C. Faleski, M. C. Marchetti, and A. A. Middleton, Vortex dynamics and defects in simulated flux flow, Phys. Rev. B **54**, 12427 (1996).

[5] K. Harada, O. Kamimura, H. Kasai, T. Matsuda, A. Tonomura, and V. V. Moshchalkov, Direct observation of vortex dynamics in superconducting films with regular arrays of defects, Science **274**, 1167 (1996).

[6] C. Reichhardt, C. J. Olson, and Franco Nori, Dynamic Phases of Vortices in Superconductors with Periodic Pinning, Phys. Rev. Lett. **78**, 2648 (1997).

[7] M.-C. Cha and H. A. Fertig, Topological defects, orientational order, and depinning of the electron solid in a random potential, Phys. Rev. B **50**, 14368 (1994).

[8] C. Reichhardt, C. J. Olson, N. Grønbech-Jensen, and F. Nori, Moving Wigner Glasses and Smectics: Dynamics of Disordered Wigner Crystals, Phys. Rev. Lett. **86**, 4354 (2001).

[9] G. Csáthy, D. Tsui, L. Pfeiffer, and K. West, Astability and Negative Differential Resistance of the Wigner Solid, Phys. Rev. Lett. **98**, 066805 (2007).

[10] T. Schulz, R. Ritz, A. Bauer, M. Halder, M. Wagner, C. Franz, C. Pfleiderer, K. Everschor, M. Garst, and A. Rosch, Emergent electrodynamics of skyrmions in a chiral magnet, Nat. Phys. **8**, 301 (2012).

[11] C. Reichhardt, D. Ray, and C. J. Olson Reichhardt, Collective Transport Properties of Driven Skyrmions with Random Disorder, Phys. Rev. Lett. **114**, 217202 (2015).

[12] C. Reichhardt and C. J. Olson, Colloidal Dynamics on Disordered Substrates, Phys. Rev. Lett. **89**, 078301 (2002).

[13] A. Pertsinidis and X. S. Ling, Statics and Dynamics of 2D Colloidal Crystals in a Random Pinning Potential, Phys. Rev. Lett. **100**, 028303 (2008).

[14] S. Deutschländer, T. Horn, H. Löwen, G. Maret, and P. Keim, Two-Dimensional Melting Under Quenched Disorder, Phys. Rev. Lett. **111**, 098301 (2013).

[15] Y. G. Cao, Q. X. Li, G. Y. Fu, J. Liu, H. Z. Guo, X. Hu, and X. J. Li, Depinning dynamics of two-dimensional magnetized colloids on a random substrate, J. Phys.: Condens. Matter **22**, 155101 (2010).

[16] P. Tierno, Depinning and Collective Dynamics of Magnetically Driven Colloidal Monolayers, Phys. Rev. Lett. **109**, 198304 (2012).

[17] A. E. Koshelev and V. M. Vinokur, Dynamic Melting of the Vortex Lattice, Phys. Rev. Lett. **73**, 3580 (1994).

[18] P. Le Doussal and T. Giamarchi, Moving glass theory of driven lattices with disorder, Phys. Rev. B **57**, 11356 (1998).

[19] L. Balents, M. C. Marchetti, and L. Radzihovsky, Nonequilibrium steady states of driven periodic media, Phys. Rev. B **57**, 7705 (1998).

[20] K. Moon, R. T. Scalettar, and G. T. Zimányi, Dynamical Phases of Driven Vortex Systems, Phys. Rev. Lett. **77**, 2778 (1996).

[21] F. Pardo, F. de la Cruz, P. L. Gammel, E. Bucher, and D. J. Bishop, Observation of smectic and moving-Bragg-glass phases in flowing vortex lattices, Nature (London) **396**, 348 (1998).

[22] C. J. Olson, C. Reichhardt, and F. Nori, Nonequilibrium Dynamic Phase Diagram for Vortex Lattices, Phys. Rev. Lett. **81**, 3757 (1998).

[23] A. C. Marley, M. J. Higgins, and S. Bhattacharya, Flux Flow Noise and Dynamical Transitions in a Flux Line Lattice, Phys. Rev. Lett. **74**, 3029 (1995).

[24] A. Kolton, D. Domínguez, and N. Grønbech-Jensen, Hall Noise and Transverse Freezing in Driven Vortex Lattices, Phys. Rev. Lett. **83**, 3061 (1999).

[25] M. C. Marchetti, A. A. Middleton, K. Saunders, and J. M. Schwarz, Driven Depinning of Strongly Disordered Media and Anisotropic Mean-Field Limits, Phys. Rev. Lett. **91**, 107002 (2003).

[26] J. Zhu, M. Li, R. Rogers, W. Meyer, R. H. Ottewill, STS-73 Space Shuttle Crew, W. B. Russel, and P. M. Chaikin, Crystallization of hard-sphere colloids in microgravity, Nature (London) **387**, 883 (1997).

[27] C. P. Royall, W. C. K. Poon, and E. R. Weeks, In search of colloidal hard spheres, Soft Matter **9**, 17 (2013).

[28] J. Bibette, F. L. Calderon, and P. Poulin, Emulsions: basic principles, Rep. Prog. Phys. **62**, 969 (1999).
[29] M. Borkovec, From micelles to microemulsion droplets: Size distributions, shape fluctuations, and interfacial tensions, J. Chem. Phys. **91**, 6268 (1989).
[30] B. E. Burkhardt, P. V. Gopalkrishnan, S. D. Hudson, A. M. Jamieson, M. A. Rother, and R. H. Davis, Droplet Growth by Coalescence in Binary Fluid Mixtures, Phys. Rev. Lett. **87**, 098304 (2001).
[31] L. Bragg and J. F. Nye, A dynamical model of a crystal structure, Proc. R. Soc. London A **190**, 474 (1947).
[32] M. Dennin, Statistics of bubble rearrangements in a slowly sheared two-dimensional foam, Phys. Rev. E **70**, 041406 (2004).
[33] M. J. Bowick, L. Giomi, H. Shin, and C. K. Thomas, Bubble-raft model for a paraboloidal crystal, Phys. Rev. E **77**, 021602 (2008).
[34] Y. Forterre and O. Pouliquen, Flows of dense granular media, Annu. Rev. Fluid Mech. **40**, 1 (2008).
[35] C. Reichhardt and C. J. Olson Reichhardt, Aspects of jamming in two-dimensional athermal frictionless systems, Soft Matter **10**, 2932 (2014).
[36] T. Bohlein, J. Mikhael, and C. Bechinger, Observation of kinks and antikinks in colloidal monolayers driven across ordered surfaces, Nature Mater. **11**, 126 (2012).
[37] J. Mikhael, J. Roth, L. Helden, and C. Bechinger, Archimedean-like tiling on decagonal quasicrystalline surfaces, Nature (London) **454**, 501 (2008).
[38] C. S. O'Hern, L. E. Silbert, A. J. Liu, and S. R. Nagel, Jamming at zero temperature and zero applied stress: The epitome of disorder, Phys. Rev. E **68**, 011306 (2003).
[39] C. J. Olson Reichhardt, E. Groopman, Z. Nussinov, and C. Reichhardt, Jamming in systems with quenched disorder, Phys. Rev. E **86**, 061301 (2012).
[40] A. L. Graves, S. Nashed, E. Padgett, C. P. Goodrich, A. J. Liu, and J. P. Sethna, Pinning Susceptibility: The Effect of Dilute, Quenched Disorder on Jamming, Phys. Rev. Lett. **116**, 235501 (2016).
[41] A. Kudrolli, M. Wolpert, and J. P. Gollub, Cluster Formation Due to Collisions in Granular Material, Phys. Rev. Lett. **78**, 1383 (1997).
[42] I. Aranson and L. Tsimring, Patterns and collective behavior in granular media: Theoretical concepts, Rev. Mod. Phys. **78**, 641 (2006).
[43] J. Tailleur and M. E. Cates, Statistical Mechanics of Interacting Run-and-Tumble Bacteria, Phys. Rev. Lett. **100**, 218103 (2008).
[44] M. E. Cates and J. Tailleur, When are active Brownian particles and run-and-tumble particles equivalent? Consequences for motility-induced phase separation, Europhys. Lett. **101**, 20010 (2013).
[45] C. Reichhardt and C. J. Olson Reichhardt, Active microrheology in active matter systems: Mobility, intermittency, and avalanches, Phys. Rev. E **91**, 032313 (2015).
[46] C. Bechinger, R. Di Leonardo, H. Löwen, C. Reichhardt, G. Volpe, and G. Volpe, Active Brownian particles in complex and crowded environments, Rev. Mod. Phys. **88**, 045006 (2016).
[47] A. Ortiz-Ambriz and P. Tierno, Engineering of frustration in colloidal artificial ices realized on midrofeatured grooved lattices, Nat. Commun. **7**, 10575 (2016).
[48] P. Tierno, Geometric Frustration of Colloidal Dimers on Honeycomb Magnetic Lattices, Phys. Rev. Lett. **116**, 038303 (2016).
[49] H. J. Zhao, V. R. Misko, and F. M. Peeters, Analysis of pattern formation in systems with competing range interactions, New J. Phys. **14**, 063032 (2012).
[50] X. B. Xu, H. Fangohr, S. Y. Ding, F. Zhou, X. N. Xu, Z. H. Wang, M. Gu, D. Q. Shi, and S. X. Dou, Phase diagram of vortex matter of type-II superconductors, Phys. Rev. B **83**, 014501 (2011).
[51] V. Moshchalkov, M. Menghini, T. Nishio, Q. H. Chen, A. V. Silhanek, V. H. Dao, L. F. Chibotaru, N. D. Zhigadlo, and J. Karpinski, Type-1.5 Superconductivity, Phys. Rev. Lett. **102**, 117001 (2009).
[52] G. Bryant, S. R. Williams, L. Qian, I. K. Snook, E. Perez, and F. Pincet, How hard is a colloidal "hard-sphere" interaction?, Phys. Rev. E **66**, 060501(R) (2002).
[53] S. Luding and H. J. Herrmann, Cluster-growth in freely cooling granular media, Chaos **9**, 673 (1999).
[54] See Supplemental Material at http://link.aps.org/supplemental/10.1103/PhysRevE.95.042902 for a video of the system with $N_p = 1440$ at a drive of $F_D/F_p = 0.2$ for $\phi = 0.3$ (pinned state) and $\phi = 0.61$ (plastic flow of clusters); for a video of the system with $N_p = 1440$ at a drive of $F_D/F_p = 1.05$ for $\phi = 0.3$ (moving chain state) and $\phi = 0.61$ (density phase separated state); for a video of the system with $N_p = 1440$ at a drive of $F_D/F_p = 2.0$ for $\phi = 0.3$ (moving chain state) and $\phi = 0.61$ (moving smectic state).
[55] C. J. Olson, C. Reichhardt, and F. Nori, Fractal Networks, Braiding Channels, and Voltage Noise in Intermittently Flowing Rivers of Quantized Magnetic Flux, Phys. Rev. Lett. **80**, 2197 (1998).
[56] J. G. Berryman, Random close packing of hard spheres and disks, Phys. Rev. A **27**, 1053 (1983).
[57] S. Torquato, Nearest-neighbor statistics for packings of hard spheres and disks, Phys. Rev. E **51**, 3170 (1995).
[58] Y. Fily and M. C. Marchetti, Athermal Phase Separation of Self-Propelled Particles with no Alignment, Phys. Rev. Lett. **108**, 235702 (2012).
[59] G. S. Redner, M. F. Hagan, and A. Baskaran, Structure and Dynamics of a Phase-Separating Active Colloidal Fluid, Phys. Rev. Lett. **110**, 055701 (2013).
[60] C. Reichhardt and C. J. Olson Reichhardt, Charge Transport Transitions and Scaling in Disordered Arrays of Metallic Dots, Phys. Rev. Lett. **90**, 046802 (2003).
[61] Y. Fily, E. Olive, N. Di Scala, and J. C. Soret, Critical behavior of plastic depinning of vortex lattices in two dimensions: Molecular dynamics simulations, Phys. Rev. B **82**, 134519 (2010).
[62] O. Pla and F. Nori, Self-Organized Critical Behavior in Pinned Flux Lattices, Phys. Rev. Lett. **67**, 919 (1991).
[63] R. M. da Silva and C. C. de Souza Silva, Vortex density waves and negative absolute resistance in patterned superconductors, Phys. Rev. B **83**, 184514 (2011).
[64] C. J. Olson Reichhardt, C. Reichhardt, and A. R. Bishop, Anisotropic sliding dynamics, peak effect, and metastability in stripe systems, Phys. Rev. E **83**, 041501 (2011).
[65] H. J. Zhao, V. R. Misko, and F. M. Peeters, Dynamics of self-organized driven particles with competing range interaction, Phys. Rev. E **88**, 022914 (2013).